

Chapter 2

Transmitter Design

Abstract This chapter gives a detailed overview of how optical high-order modulation signals are generated. It describes transmitters for the generation of optical ASK-signals, DPSK-signals and QAM-signals and considers star-shaped and square-shaped QAM constellations (Star QAM and Square QAM). Since all the transmitters are composed of fundamental key components (laser, modulators, pulse carver), the functionality of these components is discussed at the beginning of this chapter. The subsequent description of the different transmitters includes optical transmitter parts as well as electrical parts. It contains much detailed information such as the concrete assembly of the coders and level-generators. The quality of the transmitter output signals has a critical influence on the overall system performance. Therefore the electrical field for the optical output signals is analytically derived for all transmitters shown, and differences in signal characteristics, symbol transitions and chirp behavior are emphasized. This helps us understand the system behavior of the transmitters discussed later on in Chap. 7.

2.1 Transmitter Components

The following subsections briefly describe some fundamental key components of optical transmitters for high-order modulation.

2.1.1 Lasers

The ideal carrier for optical transmission is a lightwave with constant amplitude, frequency and phase. In practice, however, this perfect carrier can unfortunately not be generated. In the last decades, optical light sources have been increasingly improved. Light emitting diodes (LED) with very high spectral widths of several tens of nanometers and low output powers and multi-mode Fabry-Perot lasers with

some discrete spectral lines and a total spectral width of several nanometers can now be replaced with single-mode distributed feedback (DFB) lasers or external cavity lasers (ECL) with linewidths in the sub-MHz region. When performing direct modulation (which means that the data is modulated onto the laser drive current), the width of the emitted optical spectrum is determined by the incidental frequency modulation of the laser under amplitude modulation, often referred to as chirping of the laser, when the laser linewidth is small compared with the chirp-induced spectral broadening. To avoid this effect, external modulation can be employed. Then the laser acts as a continuous wave (CW) light source. Throughout this book, which deals with advanced modulation and detection schemes, only single-mode lasers and external modulation are considered.

The *normalized electrical field* of an ideal optical carrier as emitted from a CW laser can be expressed in complex notation as

$$\mathbf{E}_{cw}(t) = \sqrt{P_s} \cdot e^{j(\omega_s t + \varphi_s)} \cdot \mathbf{e}_s \quad (2.1)$$

In (2.1), $\sqrt{P_s}$ represents the field amplitude, $\omega_s/(2\pi)$ the frequency, φ_s the initial phase and \mathbf{e}_s the polarization of the optical carrier. The character “s” indicates the signal laser.

In practice, laser phase and amplitude noise, often called “intensity noise”, have to be taken into account. They have their origin in spontaneous emission photons which induce intensity fluctuations $\delta P(t)$ and phase fluctuations, which are represented by the signal laser phase noise $\varphi_{n_s}(t)$.

$$\mathbf{E}_{cw}(t) = \sqrt{P_s + \delta P(t)} \cdot e^{j(\omega_s t + \varphi_s + \varphi_{n_s}(t))} \cdot \mathbf{e}_s. \quad (2.2)$$

The *laser phase noise* is caused by spontaneous emission photons, not generated in phase with the stimulated emission photons but with random phase [7]. In the time domain, the evolution of the actual phase can be understood as a random walk. Within a time interval τ , the phase exhibits a random phase change of

$$\Delta\varphi_{n_s}(t) = \varphi_{n_s}(t) - \varphi_{n_s}(t - \tau). \quad (2.3)$$

Since the phase changes $\Delta\varphi_{n_s}(t)$ are caused by a high number of independent noise events—more precisely the generation of spontaneous emission photons—they can be modeled as Gaussian distributed according to the Central Limit Theorem. Furthermore, when assuming a white power spectral density of frequency noise $\dot{\varphi}_{n_s}(t)$, which represents a realistic practical assumption [8, 13], the variance of the phase change $\Delta\varphi_{n_s}(t)$ can be expressed as

$$\langle \Delta\varphi_{n_s}^2(\tau) \rangle = W_{\dot{\varphi}_{n_s}} \cdot |\tau| = \frac{2|\tau|}{t_c}, \quad (2.4)$$

where $W_{\dot{\varphi}_{n_s}}$ is the constant power spectral density of the frequency noise and t_c represents the coherence time which physically denotes the maximum delay difference up to which two components of the emitted optical field can stably interfere. When further neglecting intensity noise, the power spectral density of the optical field can be shown to exhibit the Lorentzian-shaped spectrum

$$W_{E_{cw}}(\omega) = \frac{2t_c P_s}{1 + [(\omega - \omega_s)t_c]^2}. \quad (2.5)$$

The laser linewidth of the signal laser is defined as the full-width half-maximum bandwidth of this power spectral density and is specified by

$$\Delta\nu_s = \frac{W_{\dot{\varphi}_{n_s}}}{2\pi} = \frac{1}{\pi t_c}. \quad (2.6)$$

When the laser linewidth given by (2.6) is introduced into (2.4), the variance of the phase change $\Delta\varphi_{n_s}(t)$ can be calculated by

$$\langle \Delta\varphi_{n_s}^2(\tau) \rangle = 2\pi \Delta\nu_s |\tau|, \quad (2.7)$$

showing that the phase uncertainty increases with the laser linewidth and the observed time interval. A more detailed analysis of the mechanisms and statistics of phase and frequency noise can be found in [13]. As will become clear later on in this book, laser phase noise can have a limiting effect on system performance, especially for high-order modulation formats with many phase states and when employing coherent synchronous detection.

Intensity noise can also lead to significant degradation in system performance, in particular for coherent detection with high local oscillator (LO) laser powers and when not implementing balanced detection [12, 18]. In the data sheets of laser diodes, the relative intensity noise (RIN) is usually specified. The RIN, integrated over a reference bandwidth Δf , relates the variance of the intensity fluctuations to the squared mean power:

$$\int_0^{\Delta f} RIN(f) df = \frac{\langle \delta P^2(t) \rangle}{\langle P(t) \rangle^2}. \quad (2.8)$$

The mean optical power $\langle P(t) \rangle$ is equivalent to the signal laser output power P_s or the output power of the LO laser P_{lo} , respectively, because $\langle \delta P(t) \rangle = 0$. In a simple approach, the intensity fluctuations can be modeled with Gaussian statistics and a white noise spectrum [2]. In reality, the RIN has more complex spectral characteristics, as can be observed for instance from [13, 20]. RIN values of laser diodes typically range from -160 dB/Hz to -130 dB/Hz.

2.1.2 External Optical Modulators

The optical part of high-order modulation transmitters is composed of one or more fundamental external optical modulator structures, which are briefly described in this subsection: the phase modulator (PM), the Mach-Zehnder modulator (MZM) and the optical IQ modulator (IQM). The speed attainable as well as the characteristics of the transmitter output signals depends on the properties of the technology and materials used for the modulators.

An optical *phase modulator* can be fabricated as an integrated optical device by embedding an optical waveguide in an electro-optical substrate, mostly $LiNbO_3$, see Fig. 2.1a. By utilizing the fact that the refractive index of a material, and thus the effective refractive index n_{eff} of the waveguide, can be changed by applying an external voltage via a coated electrode, the electrical field of the incoming optical carrier can be modulated in phase [20].

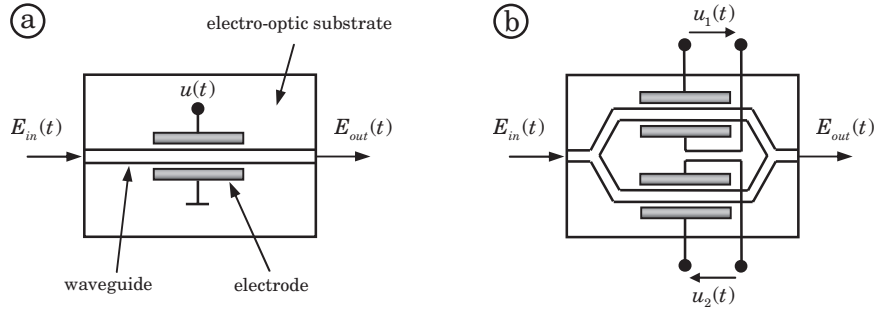


Fig. 2.1 a Integrated optical phase modulator. b Integrated optical Mach-Zehnder modulator.

Phase modulation $\varphi_{PM}(t)$ is a function of the wavelength λ , the length of the electrode l_{el} (interaction length) and the change of the effective refractive index $\Delta n_{eff}(t)$. When solely considering the Pockels effect [20], the change of the refractive index can be assumed to be linear to the applied external voltage $u(t)$.

$$\varphi_{PM}(t) = \frac{2\pi}{\lambda} \cdot \Delta n_{eff}(t) \cdot l_{el} \sim u(t) \quad (2.9)$$

In the specifications, the necessary driving voltage for achieving a phase shift of π , denoted as V_π , is typically given. Thus, the relation of the incoming optical carrier $E_{in}(t)$ and the outgoing phase modulated optical field $E_{out}(t)$, when neglecting the constant optical phase shift of the modulator, can be expressed as

$$E_{out}(t) = E_{in}(t) \cdot e^{j\varphi_{PM}(t)} = E_{in}(t) \cdot e^{j \frac{u(t)}{V_\pi} \pi}. \quad (2.10)$$

By utilizing the principle of interference, the process of phase modulation can also be used to cause an intensity modulation of the optical lightwave, when the interferometric structure shown in Fig. 2.1b is employed. This represents a dual-drive *Mach-Zehnder modulator*. In the case of dual-drive MZMs, the phase modulators in both arms can be driven independently, in contrast to single-drive MZMs. The incoming light is split into two paths, both equipped with phase modulators. After acquiring some phase differences relative to each other, the two optical fields are recombined. The interference varies from constructive to destructive, depending on the relative phase shift. Without considering the insertion loss, the transfer function of a MZM is given by

$$\frac{E_{out}(t)}{E_{in}(t)} = \frac{1}{2} \cdot \left(e^{j\varphi_1(t)} + e^{j\varphi_2(t)} \right). \quad (2.11)$$

In (2.11), $\varphi_1(t)$ and $\varphi_2(t)$ represent phase shifts in the upper and lower arms of the MZM. For a specified driving voltage to obtain a phase shift of π in the upper and lower arms, V_{π_1} and V_{π_2} , respectively, and with the driving voltages $u_1(t)$ and $u_2(t)$ as defined in Fig. 2.1b, phase shifts are related to the driving signals with

$$\varphi_1(t) = \frac{u_1(t)}{V_{\pi_1}}\pi, \quad \varphi_2(t) = \frac{u_2(t)}{V_{\pi_2}}\pi. \quad (2.12)$$

When operating the MZM in the push-push mode, which means that an identical phase shift $\varphi(t) = \varphi_1(t) = \varphi_2(t)$ is induced in both arms (for instance with $u_1(t) = u_2(t) = u(t)$ and $V_{\pi_1} = V_{\pi_2} = V_\pi$), a pure phase modulation is achieved, so that the relation between the electrical input and output field is given by (2.10) as for the simple PM. On the other hand, when one arm gets the negative phase shift of the other arm ($\varphi_1(t) = -\varphi_2(t)$, e.g. with $u_1(t) = -u_2(t) = u(t)/2$ and $V_{\pi_1} = V_{\pi_2} = V_\pi$), the MZM is operated in the push-pull mode and a chirp-free amplitude modulation is obtained. The input and output fields are then related with

$$E_{out}(t) = E_{in}(t) \cdot \cos\left(\frac{\Delta\varphi_{MZM}(t)}{2}\right) = E_{in}(t) \cdot \cos\left(\frac{u(t)}{2V_\pi}\pi\right), \quad (2.13)$$

where $\Delta\varphi_{MZM}(t) = \varphi_1(t) - \varphi_2(t) = 2\varphi_1(t)$ is the induced phase difference between the fields of the upper and lower arm. By squaring (2.13), the power transfer function of the MZM is obtained:

$$\frac{P_{out}(t)}{P_{in}(t)} = \frac{1}{2} + \frac{1}{2} \cdot \cos(\Delta\varphi_{MZM}(t)) = \frac{1}{2} + \frac{1}{2} \cdot \cos\left(\frac{u(t)}{V_\pi}\pi\right). \quad (2.14)$$

It should be noted that $u(t)$ was defined in a way that $u(t) = V_\pi$ induces a phase shift of π for the PM as well as a phase shift of π in the *power* transfer function of the MZM when it is operated in the push-pull mode.

In Fig. 2.2, two different *MZM operation principles* are illustrated. For achieving modulation in intensity, the MZM can be operated at the quadrature point, with a DC bias of $-V_\pi/2$ and a peak-to-peak modulation of V_π (see Fig. 2.2a). When the

MZM is operated at the minimum transmission point (see Fig. 2.2b), with a DC bias of $-V_\pi$ and a peak-to-peak modulation of $2V_\pi$, a phase skip of π occurs when crossing the minimum transmission point. This becomes apparent from the field transfer function. This way, the MZM can be used for binary phase modulation and for modulation of the field amplitude in each branch of an optical IQ modulator.

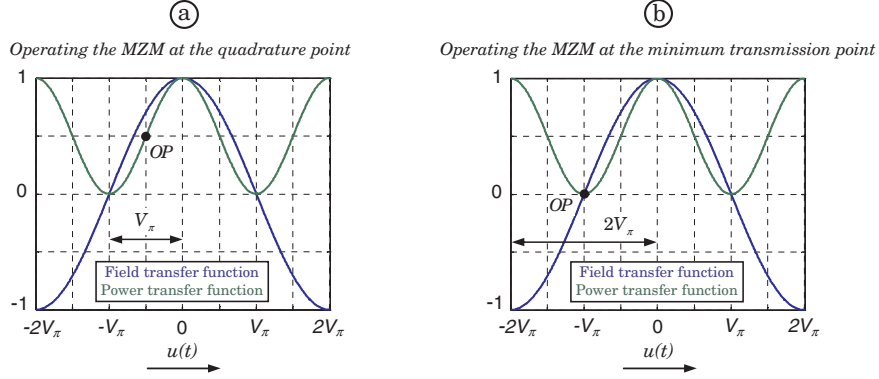


Fig. 2.2 Operating the MZM in the quadrature point (a) and the minimum transmission point (b)

Mach-Zehnder modulators can be implemented in Lithium Niobate ($LiNbO_3$), Gallium Arsenide ($GaAs$) and Indium Phosphide (InP) [23]. Typical V_π driving voltages range from approximately 3 V to about 6 V.

A third fundamental modulator structure is the *optical IQ modulator*. It can be composed of a PM and two MZMs, and is commercially available in an integrated form [1]. As illustrated in Fig. 2.3a, the incoming light is equally split into two arms, the in-phase (I) and the quadrature (Q) arm. In both paths, a field amplitude modulation is performed by operating the MZMs in the push-pull mode at the minimum transmission point. Moreover, a relative phase shift of $\pi/2$ is adjusted in one arm, for instance by an additional PM. This way, any constellation point can be reached in the complex IQ-plane after recombining the light of both branches (see Fig. 2.3b). Within the IQ modulator pictured in Fig. 2.3a, the induced phase differences of the MZMs in the upper and lower paths are

$$\Delta\varphi_I(t) = \frac{u_I(t)}{V_\pi}\pi, \quad \Delta\varphi_Q(t) = \frac{u_Q(t)}{V_\pi}\pi. \quad (2.15)$$

When neglecting any insertion loss and setting the driving voltage of the PM to $u_{PM} = -V_\pi/2$, the field transfer function of the IQM can be expressed as

$$\frac{E_{out}(t)}{E_{in}(t)} = \frac{1}{2} \cos\left(\frac{\Delta\varphi_I(t)}{2}\right) + j \frac{1}{2} \cos\left(\frac{\Delta\varphi_Q(t)}{2}\right). \quad (2.16)$$

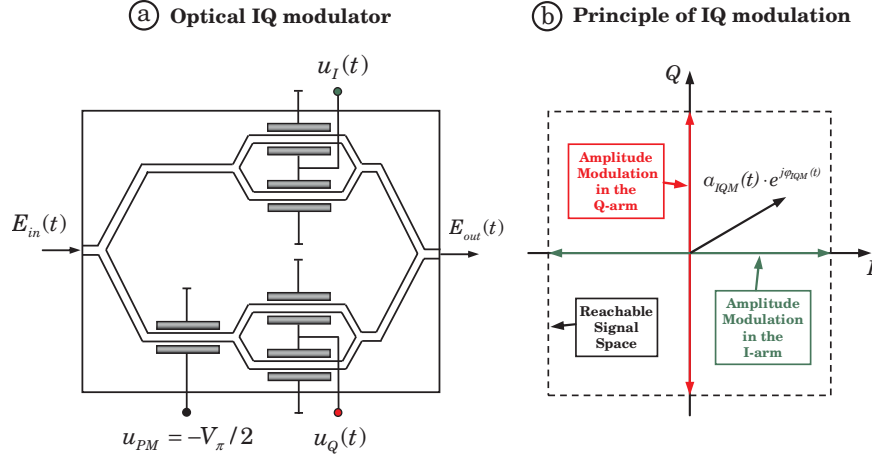


Fig. 2.3 a Optical IQ modulator. b Principle of IQ modulation.

By using (2.15) and (2.16), the amplitude modulation $a_{IQM}(t)$ and the phase modulation $\phi_{IQM}(t)$, performed by the IQM, can be calculated by

$$a_{IQM}(t) = \left| \frac{E_{out}(t)}{E_{in}(t)} \right| = \frac{1}{2} \sqrt{\cos^2 \left(\frac{u_I(t)}{2V_\pi} \pi \right) + \cos^2 \left(\frac{u_Q(t)}{2V_\pi} \pi \right)}, \quad (2.17)$$

$$\phi_{IQM}(t) = \arg \left[\cos \left(\frac{u_I(t)}{2V_\pi} \pi \right), \cos \left(\frac{u_Q(t)}{2V_\pi} \pi \right) \right]. \quad (2.18)$$

In (2.18), the $\arg [I, Q]$ operation denotes the calculation of the angle of a complex value from the real and imaginary parts in the range between $-\pi$ and π .

2.1.3 Pulse Carvers and Impulse Shapers

The shape of the transmitted optical pulses significantly affects the overall performance of optical fiber transmission systems. The pulse shape used in most commercial systems is NRZ, where a pulse filling the entire bit slot is transmitted for all symbols with non-zero power. The power does not always go to zero when passing from one symbol to another. In the case of RZ pulses, the optical power goes to zero within each symbol period. Therefore, power is smaller during the symbol transitions and the undesired frequency modulation (chirp) arising during the phase transitions can not take effect or is at least reduced, depending on the optical pulse width and the rise time of the electrical driving signals.

Optical signals with RZ pulse shape can be created either by electronically generating RZ waveforms or by carving RZ pulses in the optical domain, using an extra optical pulse carver. When employing the latter method, RZ pulses with a duty cycle of 50% can be generated with a MZM, which is operated at the quadrature point and driven with a sinusoidal electrical signal with a peak-to-peak amplitude of V_π , a frequency corresponding to the symbol rate $r_S = 1/T_S$ and a phase offset of $-\pi/2$. The electrical driving signal is given by $u(t) = V_\pi/2 \cdot \sin(2\pi t/T_S - \pi/2) - V_\pi/2$, where T_S denotes the duration of one symbol.

The field transfer function of the *optical RZ pulse carver* for generating RZ pulses with a duty cycle of 50% is defined as

$$\frac{E_{out}(t)}{E_{in}(t)} = \cos \left[\frac{\pi}{4} \cdot \sin \left(2\pi \frac{t}{T_S} - \frac{\pi}{2} \right) - \frac{\pi}{4} \right]. \quad (2.19)$$

Even when employing optical pulse carving, the final optical pulse form at the transmitter output depends also on the shape of the electrical driving signals. These can be formed by *electrical impulse shapers* (IS) before feeding into the modulator driving electrodes. In system simulations, electrical pulses without overshoots and with specified rise times can be generated by filtering a rectangular input time function with a non-causal linear time invariant filter with the Gaussian shaped impulse response

$$h(t) = \frac{2}{\sqrt{\pi} T_e} \cdot e^{-(2t/T_e)^2}. \quad (2.20)$$

The resulting output pulse of the electrical impulse shaper is given by the convolution of the rectangular signal with the impulse response $h(t)$ and is specified by

$$p(t) = \frac{1}{2} \cdot \left[\operatorname{erfc} \left(\frac{2(t - T_S)}{T_e} \right) - \operatorname{erfc} \left(\frac{2t}{T_e} \right) \right]. \quad (2.21)$$

In (2.20) and (2.21), T_e represents the filter time constant, which can be approximately related to the electrical rise time Δt as

$$\Delta t \approx \frac{3}{4} T_e, \quad (2.22)$$

as long it is assumed that the symbol time T_S is much longer than the filter time constant T_e [2].

Having now discussed some fundamental components used in the various transmitters for high-order modulation, some basics for multi-level signaling are briefly presented in Sect. 2.2. Afterwards, the transmitters for particular modulation formats are described in detail.

2.2 Multi-Level Signaling

In digital optical transmission with high-order modulation, m data bits, denoted here as $\{b_{1k}, b_{2k}, \dots, b_{mk}\}$, are collected and mapped to a complex symbol b_k chosen from an alphabet A of elements A_n ($n = 1..M$, $M = 2^m$). Each symbol b_k can be interpreted as a complex phasor with the in-phase and quadrature coordinates b_k^i and b_k^q , respectively,

$$b_k = b_k^i + jb_k^q, \quad (2.23)$$

and with amplitude and phase states given by

$$a_{b_k} = \sqrt{b_k^{i^2} + b_k^{q^2}}, \quad \varphi_{b_k} = \arg [b_k^i, b_k^q]. \quad (2.24)$$

One of the $M = 2^m$ symbols is assigned to each symbol interval (denoted by the integer k , which has a range of 1 to ∞) of length $T_S = m \cdot T_B$, where $r_B = 1/T_B$ is the data rate. The assignment of respective combinations of m bits to symbols with particular amplitude and phase states (bit mapping) is defined in a so called “constellation diagram”. For the best optical signal to noise ratio (OSNR) performance, bit mapping should be arranged so that only one bit per symbol differs from a neighboring symbol (Gray coding). The symbols are transmitted on the reduced symbol rate $r_S = 1/T_S = r_B/m$.

For the theoretical description of the electrical driving signals in Sect. 2.6, the in-phase and quadrature symbol coordinates are scaled to unity, limiting the maximum coordinates of the I-axis and Q-axis to one. These normalized in-phase and quadrature coordinates are denoted as i_k and q_k throughout this book. By scaling the symbol coordinates b_k^i and b_k^q to unity, the normalized in-phase and quadrature coordinates i_k and q_k can be expressed as

$$i_k = \frac{b_k^i}{b_{max}^i}, \quad q_k = \frac{b_k^q}{b_{max}^q}, \quad (2.25)$$

where b_{max}^i and b_{max}^q are given by

$$b_{max}^i = \max_n \{ |Re \{A_n\}| \}, \quad b_{max}^q = \max_n \{ |Im \{A_n\}| \}. \quad (2.26)$$

The relation between i_k and q_k and the data bits is specified by the bit mapping used respectively and illustrated more precisely later on.

2.3 ASK Transmitters

The most simple optical multi-level signaling scheme is the M -ary ASK, where information is encoded into several intensity levels. The *binary* ASK (2ASK), usually

denoted as OOK, is the standard modulation format in commercially deployed optical transmission systems. The 2ASK constellation diagram defines only two symbol points. Just one bit b_{1k} is assigned to each symbol, as it is depicted in Fig. 2.4b. Figure 2.4a shows a 2ASK transmitter when performing external modulation.

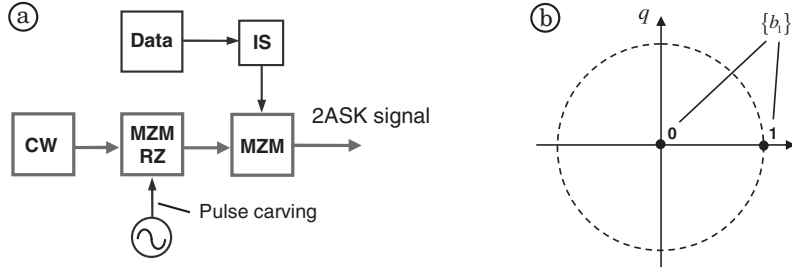


Fig. 2.4 a 2ASK transmitter with external modulation. b 2ASK constellation diagram.

The optical part consists of a CW laser, an optional MZM for RZ pulse carving and a MZM for intensity modulation, which is operated at the quadrature point. A nice side effect of using a MZM for intensity modulation, is the nonlinear compression of the MZM transfer function at high and low transmission, which can suppress ripples on electrical driving signals.

The electrical data signal can be formed by an impulse shaper as explained in Sect. 2.1.3. The optical transmitter output signal for RZ-ASK, when neglecting laser noises and polarization, can be described by

$$E_s(t) = \sqrt{P_s} \cdot e^{j(\omega_s t + \varphi_s)} \cdot \cos\left(\frac{u(t)}{2V_\pi} \pi\right) \cdot \cos\left(\frac{\pi}{4} \sin\left(2\pi \frac{t}{T_S} - \frac{\pi}{2}\right) - \frac{\pi}{4}\right), \quad (2.27)$$

whereas the second cosine-term disappears in the case of NRZ. The electrical driving signal for 2ASK is defined as

$$u(t) = -V_\pi + V_\pi \cdot \sum_k (b_{1k} \cdot p(t - kT_S)), \quad b_{1k} \in \{0, 1\}. \quad (2.28)$$

High-order ASK formats have been investigated in [21] and [24] where it was shown that they require high signal to noise ratios for direct detection, especially in optically amplified links due to the intensity dependence of the signal-ASE noise. In principle, they can be generated with the same optical transmitter. However, multi-level electrical signals would have to be produced by an adequate electrical driving circuit to drive the MZM.

The generation of multi-level electrical driving signals is quite challenging for high data rates because the *eye spreading* increases when overlapping different binary electrical signals to create a multi-level signal, which leads to a degradation of the system performance. The eye-spreading can be defined as $\Delta_e = (\delta_1 + \delta_2)/d_e$,

where δ_1 and δ_2 describe the ripples (or the spreadings) in the upper and lower levels and d_e is the height of the eye diagram, as shown in Fig. 2.5. For instance, if two binary signals are summed to a quaternary signal, the eye spreading is increased by a factor of three [6].

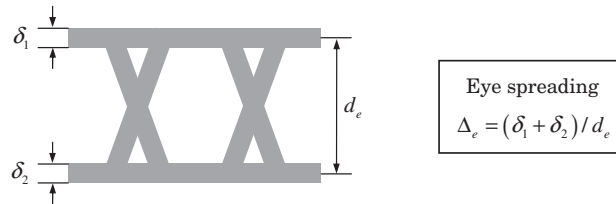


Fig. 2.5 Definition of eye spreading for a binary signal, based on [6]

2.4 DPSK Transmitters

Figure 2.6 shows constellation diagrams of different DPSK formats. All the constellation points lie in one circle. *Bit mapping* can theoretically be chosen arbitrarily. Here it is arranged in Gray code, so that only one bit per symbol differs from a neighboring symbol, leading to the best noise performance.

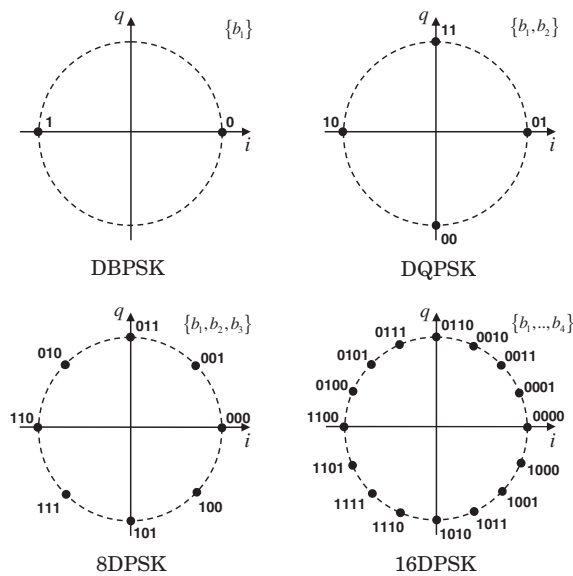


Fig. 2.6 DPSK constellation diagrams with Gray coded bit mappings

Basically, optical DPSK signals can be constituted by many different transmitter types. Optical complexity can be reduced through increased electrical complexity and vice versa. A single PM or MZM in the optical part would be sufficient to generate arbitrary DPSK signals. However, multi-level electrical driving signals are required for high-order DPSK formats in that case. Their generation increases the electrical effort and is problematic due to the eye spreading problem. Another option is to use an optical IQ modulator alone. In this situation, the necessary number of states of electrical driving signals corresponds to the number of projections of the symbols to the I-axis and the Q-axis. From a practical point of view, the IQ modulator is not the best choice for generating high-order DPSK signals because all constellation points lie in one circle, and the distances between the signal states of the in-phase and quadrature driving signals are short.

The discussion of DPSK transmitters within this book is restricted to configurations which require solely binary electrical driving signals. In Sect. 2.4.1 and Sect. 2.4.2, respectively, two different configurations are presented which are denoted here as “serial DPSK transmitter” and “parallel DPSK transmitter”.

2.4.1 Serial DPSK Transmitter

One way of generating optical DPSK signals with binary electrical driving signals is to use m consecutive PMs, where m is the number of bits per symbol. This transmitter is shown in Fig. 2.7, and is called *serial transmitter* throughout this book. After the first PM (phase shift π), a DBPSK signal is obtained. After the second PM (phase shift $\pi/2$) a DQPSK signal is obtained, and so on.

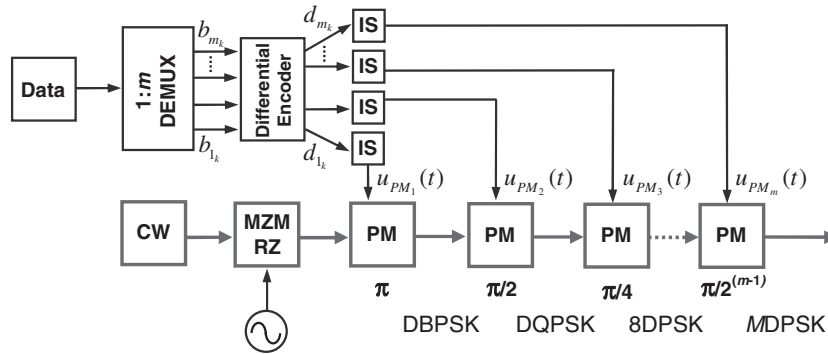


Fig. 2.7 DPSK transmitter with binary electrical driving signals, serial configuration

In the electrical part of the transmitter, the data signal is first parallelized with a $1:m$ demultiplexer. Parallelized data bits $\{b_{1_k}, b_{2_k}, \dots, b_{m_k}\}$ are then fed into a differential DPSK encoder, whose complexity and configuration generally depends on the order of the DPSK modulation, the structure of the optical transmitter part, as well as the used bit mapping of the data to the constellation points. The differential encoding is performed to enable differential detection, or to resolve phase ambiguity arising from carrier synchronization at the receiver (as described in Sect. 3.5). When employing synchronous detection techniques without differential decoding, the differential encoder can be omitted and only PSK signals generated. The functionality of the differential encoders is discussed in more detail in Sect. 2.4.3.

At the differential encoder's outputs, the encoded output data $\{d_{1_k}, d_{2_k}, \dots, d_{m_k}\}$ is obtained and passed to electrical impulse shapers and subsequently to the optical modulators as illustrated in Fig. 2.7. The NRZ output signal of the serial DPSK transmitter for a DPSK format with m bits per symbol is given by

$$E_s(t) = \sqrt{P_s} \cdot e^{j(\omega_s t + \varphi_s)} \cdot e^{j \frac{u_{PM_1}(t)}{V_\pi} \pi} \cdot e^{j \frac{u_{PM_2}(t)}{V_\pi} \pi} \cdot \dots \cdot e^{j \frac{u_{PM_m}(t)}{V_\pi} \pi}, \quad (2.29)$$

with the binary electrical driving voltages

$$u_{PM_n}(t) = \frac{V_\pi}{2^{n-1}} \cdot \sum_k (d_{n_k} \cdot p(t - kT_S)), \quad (2.30)$$

where $n = \{1, 2, \dots, m\}$, and $d_{n_k} \in \{0, 1\}$ represents the n -th differentially encoded bit of a symbol consisting of m bits in the k -th symbol interval.

2.4.2 Parallel DPSK Transmitter

A second DPSK transmitter configuration, which also uses binary electrical driving signals, is composed of a combination of an optical IQ modulator and consecutive phase modulators, in the following called *parallel transmitter* and depicted in Fig. 2.8. The optical IQ modulator accomplishes a DQPSK modulation, and higher-order DPSK signals are generated by the consecutive PMs.

The electrical transmitter part is identical to the one for the serial transmitter, with the exception of the internal setup of the differential encoder. To accomplish DQPSK modulation, the Mach-Zehnder modulators in the I-arm and the Q-arm of the IQM are operated at the minimum transmission point and driven by binary electrical driving signals

$$u_I(t) = -2V_\pi + 2V_\pi \cdot \sum_k (d_{1_k} \cdot p(t - kT_S)), \quad (2.31)$$

$$u_Q(t) = -2V_\pi + 2V_\pi \cdot \sum_k (d_{2_k} \cdot p(t - kT_S)). \quad (2.32)$$

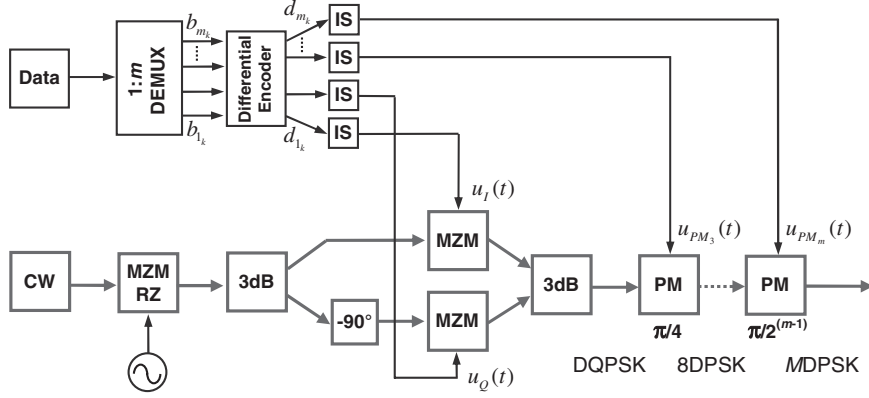


Fig. 2.8 Parallel DPSK transmitter with binary electrical driving signals

The driving signals of the consecutive phase modulators are defined by (2.30) for $n = \{3..m\}$. The optical output signal of the parallel DPSK transmitter for NRZ line coding is specified by

$$E_s(t) = \sqrt{P_s} \cdot e^{j(\omega_s t + \varphi_s)} \cdot a_{IQM}(t) \cdot e^{j\varphi_{IQM}(t)} \cdot e^{j \frac{u_{PM_3}(t)}{V_\pi} \pi} \cdot \dots \cdot e^{j \frac{u_{PM_m}(t)}{V_\pi} \pi}, \quad (2.33)$$

where $a_{IQM}(t)$ and $\varphi_{IQM}(t)$ describe the amplitude and phase modulation of the IQM, given by (2.17) and (2.18), respectively, and the parameter V_π is assumed to be the same for all the modulators used, for simplicity.

2.4.3 Differential Encoding

In the differential encoder, the data bits $\{b_{1_k}, b_{2_k}, \dots, b_{m_k}\}$, which are mapped to symbols as defined by the original bit mapping, for instance the Gray coded bit mapping in Fig. 2.6, are encoded in a way to represent phase *differences*. To achieve this, appropriate absolute phase states φ_k must be adjusted at the encoder output for given phase differences φ_{b_k} and previously given absolute phase states φ_{k-1} according to $\varphi_k = \varphi_{k-1} + \varphi_{b_k}$. The symbol assignment at the encoder output, which describes the mapping of the differentially encoded bits $\{d_{1_k}, d_{2_k}, \dots, d_{m_k}\}$ into symbols with absolute phase states φ_k , must be defined according to a particular optical transmitter configuration in order to drive the optical modulators adequately to obtain the desired absolute phase states.

Different symbol assignments are appropriate at the encoder output for the serial and the parallel DPSK transmitter, as shown in Fig. 2.9. Therefore different encoders are needed for each of the two configurations. For the serial transmitter, the symbol assignment must be arranged in chronologically increasing order, as illustrated in

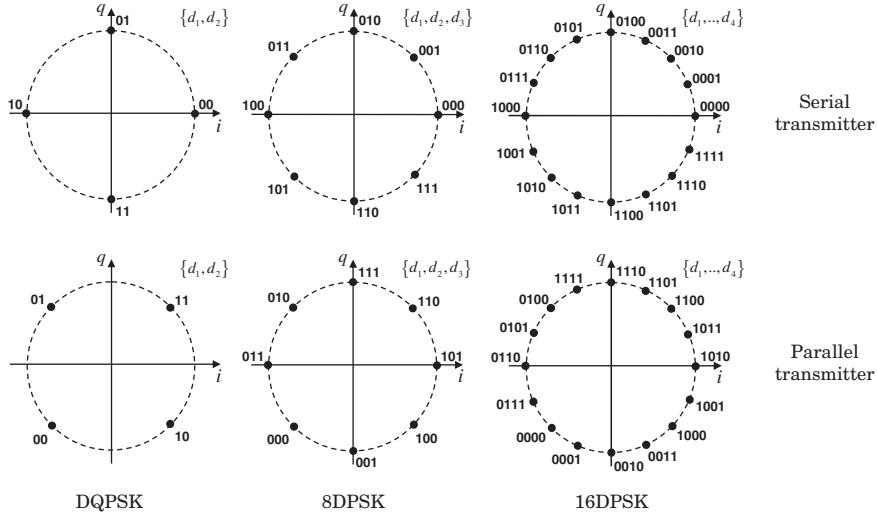


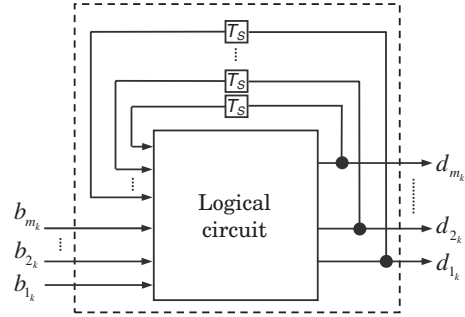
Fig. 2.9 Symbol assignment to absolute phase states at the differential encoder output for the serial DPSK transmitter (*top*) and the parallel DPSK transmitter (*bottom*)

the upper part of Fig. 2.9 for DQPSK, 8DPSK and 16DPSK, respectively. As regards the parallel transmitter, the symbols must be assigned differently. For instance, when driving the MZM in the I-arm and the Q-arm of the IQM, each with a logical one, an optical phase of $\pi/4$ is obtained, in contrast to the serial configuration, where an optical phase of $3/2 \cdot \pi$ results for driving both PMs with a logical one. The symbol assignment for the parallel transmitter used here is shown in the bottom part of Fig. 2.9 for DQPSK, 8DPSK and 16DPSK, respectively. Because the absolute phase is not relevant for differential detection, the symbol assignments can also be arbitrarily rotated for both transmitters.

In any differential encoder, the data bits of the current symbol $\{b_{1k}, b_{2k}, \dots, b_{mk}\}$, representing the current phase difference, are combined with the previous encoder output bits $\{d_{1k-1}, d_{2k-1}, \dots, d_{mk-1}\}$, representing the absolute optical phase of the previous symbol, in a logical circuit, in order to specify the next encoder output bits $\{d_{1k}, d_{2k}, \dots, d_{mk}\}$ which define the current optical phase. The general structure of a differential encoder is depicted in Fig. 2.10.

The following paragraphs derive logical relations which characterize the logical circuit of the differential encoders for different DPSK transmitters. They are only valid for employing the Gray coded bit mapping to phase differences and the symbol assignment to absolute phases as defined in Fig. 2.6 and Fig. 2.9, respectively. Other mappings are possible, but would yield other relations.

Fig. 2.10 General structure of a differential encoder



Differential Encoders for DBPSK and DQPSK

In the case of *DBPSK*, differential encoding can be achieved easily. A logical one in the current data indicates a phase change of π . By combining the current data bit with the previous encoder output bit in a simple XOR gate, the next encoder output bit is obtained.

The encoders required within *DQPSK* transmitters are yet more complex. They have to provide two output bits d_{1k} and d_{2k} , which depend on the input data bits b_{1k} and b_{2k} , as well as on the previous encoder output bits d_{1k-1} and d_{2k-1} . Within the *serial transmitter*, the encoder output signals are taken to drive the two PMs. The first PM changes the phase between 0 and π , and the second one changes the phase between 0 and $\pi/2$. In this way, the four absolute phase states 0, $\pi/2$, π , and $3/2 \cdot \pi$ can be adjusted with a symbol assignment in chronologically increasing order. The truth table for the DQPSK encoder of the serial transmitter is given by Table 2.1.

Table 2.1 Truth table for the differential encoder appropriate for the serial DQPSK transmitter

d_{1k}	d_{2k}	φ_k	d_{1k-1}	d_{2k-1}	φ_{k-1}	b_{1k}	b_{2k}	φ_{b_k}
0	0	0	0	0	0	0	1	0
0	0	0	0	1	$\pi/2$	0	0	$3/2 \cdot \pi$
0	0	0	1	0	π	1	0	π
0	0	0	1	1	$3/2 \cdot \pi$	1	1	$\pi/2$
0	1	$\pi/2$	0	0	0	1	1	$\pi/2$
0	1	$\pi/2$	0	1	$\pi/2$	0	1	0
0	1	$\pi/2$	1	0	π	0	0	$3/2 \cdot \pi$
0	1	$\pi/2$	1	1	$3/2 \cdot \pi$	1	0	π
1	0	π	0	0	0	1	0	π
1	0	π	0	1	$\pi/2$	1	1	$\pi/2$
1	0	π	1	0	π	0	1	0
1	0	π	1	1	$3/2 \cdot \pi$	0	0	$3/2 \cdot \pi$
1	1	$3/2 \cdot \pi$	0	0	0	0	0	$3/2 \cdot \pi$
1	1	$3/2 \cdot \pi$	0	1	$\pi/2$	1	0	π
1	1	$3/2 \cdot \pi$	1	0	π	1	1	$\pi/2$
1	1	$3/2 \cdot \pi$	1	1	$3/2 \cdot \pi$	0	1	0

By using Karnaugh maps, for instance, the logical relations for the encoder output bits d_{1k} and d_{2k} can easily be derived from Table 2.1 for the serial transmitter:

$$d_{1k} = \overline{b_{2k}} \overline{d_{1k-1}} \overline{d_{2k-1}} + b_{1k} \overline{d_{1k-1}} d_{2k-1} + \overline{b_{1k}} d_{1k-1} d_{2k-1} + b_{2k} d_{1k-1} \overline{d_{2k-1}}, \quad (2.34)$$

$$d_{2k} = \overline{b_{1k}} \overline{b_{2k}} \overline{d_{2k-1}} + \overline{b_{1k}} b_{2k} d_{2k-1} + b_{1k} b_{2k} \overline{d_{2k-1}} + b_{1k} \overline{b_{2k}} d_{2k-1}. \quad (2.35)$$

In (2.34) and (2.35), “+” denotes logical OR, the particular terms are associated by logical AND, and the “overlines” indicate logical negation. In practice, the encoder can be implemented using the adequate AND and OR gates.

Due to the different symbol assignment at the encoder output, the differential encoder of the *parallel transmitter* differs from the one of the serial transmitter. Its truth table is shown in Table 2.2. The corresponding logical relations for the two encoder output bits d_{1k} and d_{2k} for the parallel DQPSK transmitter are

$$d_{1k} = b_{1k} \overline{d_{1k-1}} \overline{d_{2k-1}} + \overline{b_{2k}} \overline{d_{1k-1}} d_{2k-1} + \overline{b_{1k}} d_{1k-1} d_{2k-1} + b_{2k} d_{1k-1} \overline{d_{2k-1}}, \quad (2.36)$$

$$d_{2k} = \overline{b_{2k}} \overline{d_{1k-1}} \overline{d_{2k-1}} + \overline{b_{1k}} \overline{d_{1k-1}} d_{2k-1} + b_{2k} d_{1k-1} d_{2k-1} + b_{1k} d_{1k-1} \overline{d_{2k-1}}. \quad (2.37)$$

Table 2.2 Truth table for the differential encoder appropriate for the parallel DQPSK transmitter

d_{1k}	d_{2k}	φ_k	d_{1k-1}	d_{2k-1}	φ_{k-1}	b_{1k}	b_{2k}	φ_{bk}
0	0	$5/4 \cdot \pi$	0	0	$5/4 \cdot \pi$	0	1	0
0	0	$5/4 \cdot \pi$	0	1	$3/4 \cdot \pi$	1	1	$\pi/2$
0	0	$5/4 \cdot \pi$	1	0	$7/4 \cdot \pi$	0	0	$3/2 \cdot \pi$
0	0	$5/4 \cdot \pi$	1	1	$\pi/4$	1	0	π
0	1	$3/4 \cdot \pi$	0	0	$5/4 \cdot \pi$	0	0	$3/2 \cdot \pi$
0	1	$3/4 \cdot \pi$	0	1	$3/4 \cdot \pi$	0	1	0
0	1	$3/4 \cdot \pi$	1	0	$7/4 \cdot \pi$	1	0	π
0	1	$3/4 \cdot \pi$	1	1	$\pi/4$	1	1	$\pi/2$
1	0	$7/4 \cdot \pi$	0	0	$5/4 \cdot \pi$	1	1	$\pi/2$
1	0	$7/4 \cdot \pi$	0	1	$3/4 \cdot \pi$	1	0	π
1	0	$7/4 \cdot \pi$	1	0	$7/4 \cdot \pi$	0	1	0
1	0	$7/4 \cdot \pi$	1	1	$\pi/4$	0	0	$3/2 \cdot \pi$
1	1	$\pi/4$	0	0	$5/4 \cdot \pi$	1	0	π
1	1	$\pi/4$	0	1	$3/4 \cdot \pi$	0	0	$3/2 \cdot \pi$
1	1	$\pi/4$	1	0	$7/4 \cdot \pi$	1	1	$\pi/2$
1	1	$\pi/4$	1	1	$\pi/4$	0	1	0

Differential Encoders for Higher-Order DPSK Formats

In the same manner, one can specify differential encoders for the higher-order DPSK transmitters. Starting from the constellation diagrams with bit mappings and symbol assignments defined in Fig. 2.6 and Fig. 2.9, respectively, truth tables can be established. Subsequently, the corresponding Karnaugh maps can be evaluated in order to determine the logical relations of the encoders.

Since the equations resulting for 8DPSK and 16DPSK are quite bulky, they are given in Appendix A. It becomes apparent here that the complexity of the differential encoder grows significantly with the increasing order of the phase modulation. For 16DPSK, the differential encoder is very complex. For instance, the relation for the encoder output bit d_{1k} has 30 OR combined terms, each consisting of 4-7 AND combined inputs.

Now having provided all the relevant functional information about the setup of the serial and parallel DPSK transmitters, the following subsection discusses the properties of their output signals.

2.4.4 Signal Properties

The structure of the transmitter affects the signal characteristics and the transmission properties of the generated optical DPSK signals, due to the fact that the symbol transitions (amplitude and phase transitions) of the transmitters are different, especially in the case of NRZ. An optical high-order modulation signal at the transmitter output can be generally described by

$$E_s(t) = \sqrt{P_s} \cdot e^{j(\omega_s t + \varphi_s)} \cdot a(t) \cdot e^{j\varphi(t)}, \quad (2.38)$$

where $A(t) = a(t) \cdot e^{j\varphi(t)}$ represents the normalized complex modulation envelope of the optical signal with time dependent amplitude $a(t)$ and phase $\varphi(t)$. The squared amplitude $a^2(t)$ times the CW laser power P_s represents the instantaneous signal power (which is proportional to the signal intensity). Another important parameter, which has a significant influence on the transmission performance, is the derivative of the optical phase $\dot{\varphi}(t) = d\varphi(t)/dt$. It is a measure for the undesired frequency modulation occurring during the symbol transitions, usually denoted as chirp.

The complex envelope of the DPSK transmitter output signals can be extracted from (2.29) and (2.33). The normalized *intensity eyes*, the *IQ diagrams* ($Im\{A(t)\}$ versus $Re\{A(t)\}$, where $a(t)$ is scaled here to unity for illustration purposes) and the *chirp characteristics* are plotted for both transmitter types discussed above and both pulse shapes for 8DPSK modulation in Fig. 2.11, assuming a data rate of 40 Gbit/s and an electrical rise time of 1/4 of the symbol duration.

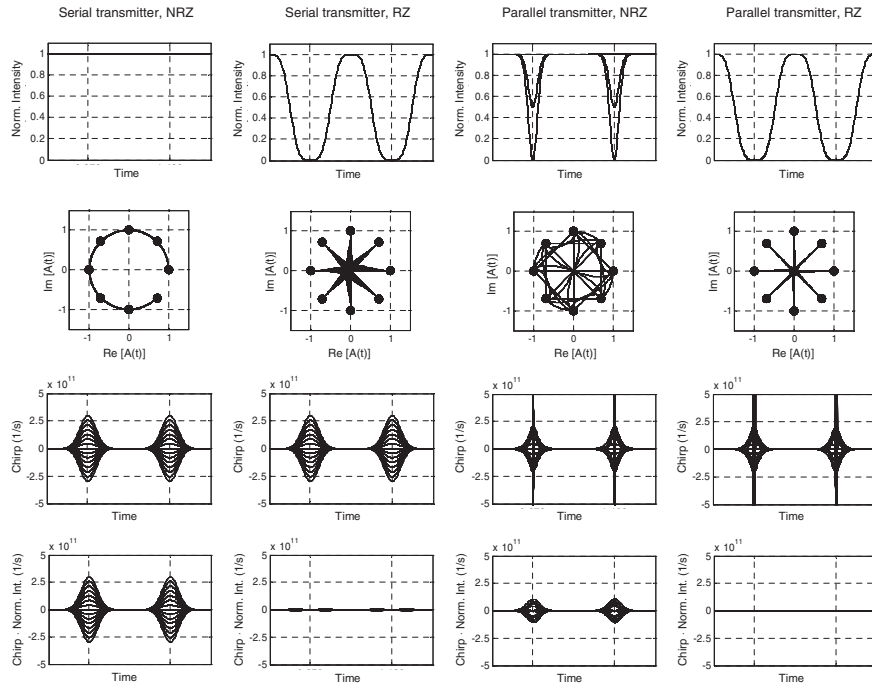


Fig. 2.11 Optical signal properties of different 8DPSK transmitters

When the serial transmitter and NRZ pulse shape are employed, symbol transitions are conducted on circles, and there is constant power during phase changes. Chirp appears during the symbol transitions, and its magnitude depends on the steepness of the phase jumps. An intuitive measure for the disturbing effect of the chirp during transmission is the product of the chirp and the intensity as is shown in the bottom eye diagrams of Fig. 2.11. It becomes apparent that the chirp has a strong effect for the serial transmitter and NRZ pulse shape, due to permanent full power. In the case of RZ, there is almost no optical power during phase changes, and only a very small residual impact of the chirp can be determined. For the parallel transmitter, the impact of the chirp is reduced even for the NRZ pulse shape. The symbol transitions are different due to the usage of an IQ modulator, and power is reduced for some transitions (intensity dips). The chirp shows high peaks when the point of origin is crossed in the IQ diagram (the phase jumps abruptly by $\pm\pi$). However this is not problematic because no optical power exists at this moment. The product of the chirp and the intensity is clearly reduced compared with the serial NRZ transmitter, so a better transmission performance can be expected.

2.5 Star QAM Transmitters

When compared with pure phase modulation, combined phase and amplitude modulation (quadrature amplitude modulation, QAM) exhibits a reduced number of phase states for the same number of symbols. The constellation points can be arranged in a square (Square QAM formats) or they can lie on multiple circles (Star QAM formats). The phases are arranged with equal spacing for Star QAM formats, as shown for Star 16QAM in Fig. 2.13, so the phase difference of any two symbols corresponds to a phase state defined in the constellation diagram and phase information can be differentially encoded as for DPSK formats. Thus, Star QAM signals with differentially encoded phases are suitable to be detected by receivers with differential detection. By contrast, Square QAM signals are conveniently detected by coherent synchronous receivers, but can also be detected by differential detection when phase pre-integration is employed at the transmitter [9].

To accomplish the generation of Star QAM signals with differentially encoded phases, the same equipment can be used as for DPSK transmitters just described. The DPSK transmitters—in serial or parallel configuration—only have to be extended by an additional MZM for intensity modulation, to be able to place symbols on different intensity rings.

In principle, arbitrary Star QAM constellations are possible. The Star 8QAM format (2ASK-DQPSK) was investigated in [11]. A Star 8QAM transmitter can be composed of a DQPSK transmitter followed by an additional MZM and can use the same differential encoders as a DQPSK transmitter. The transmitter for Star 16QAM (2ASK-8DPSK) consists of an 8DPSK transmitter, extended by a MZM for intensity modulation, as shown in Fig. 2.12 for the serial configuration.

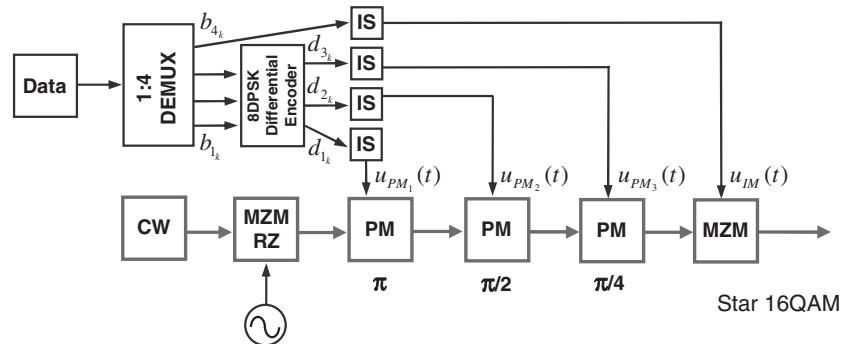


Fig. 2.12 Optical Star 16QAM transmitter with differential phase encoding, serial configuration

Figure 2.13 illustrates the Star 16QAM constellation diagrams with Gray coded bit mapping (Fig. 2.13a) and symbol assignments at the encoder output for the serial and parallel transmitters (Fig. 2.13b and Fig. 2.13c).

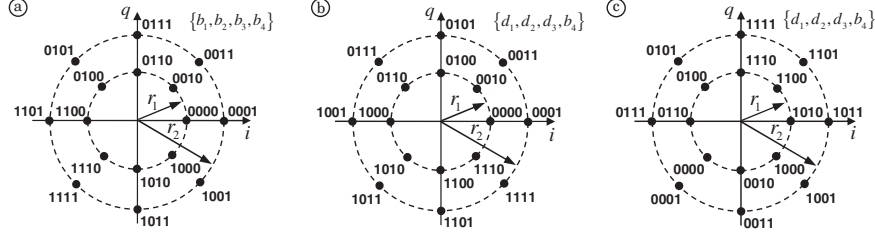


Fig. 2.13 Star 16QAM Gray coded original bit mapping (a) and symbol assignments at the encoder output for the serial transmitter (b) as well as the parallel transmitter (c)

As for 16DPSK, four bits are mapped to one symbol. However, high spectral efficiency can be obtained here without using the very complex differential 16DPSK encoder. Instead, 8DPSK encoders can be employed. When compared with 8DPSK, the constellation diagram consists of a second circle with eight more symbols. The fourth bit b_{4k} indicates if a symbol belongs to the inner or the outer circle and is used to drive the additional MZM.

One degree of freedom which can optimize the OSNR performance for Star QAM formats with only two amplitude states, is the *ring ratio* $RR = r_2/r_1$, where r_1 and r_2 are the amplitudes of the inner and outer circle, respectively, as illustrated in Fig. 2.13. The influence of the ring ratio on the OSNR performance is discussed later on in the second part of this book.

Another Star QAM constellation with 16 symbols, composed of four amplitude and four phase states (4ASK-DQPSK), has been investigated in [19]. The definition of only four phase states has the advantage that data recovery is easier to accomplish for differential detection. On the other hand, the use of more than two amplitude states leads to high OSNR requirements for intensity detection and therefore to a poor overall OSNR performance.

Generally, when using the *serial NRZ-Star QAM transmitter*, an optical Star QAM signal with only two amplitude states can be mathematically described by

$$E_s(t) = \sqrt{P_s} \cdot e^{j(\omega_s t + \varphi_s)} \cdot e^{j \frac{u_{PM_1}(t)}{V_\pi} \pi} \cdot \dots \cdot e^{j \frac{u_{PM_{m-1}}(t)}{V_\pi} \pi} \cdot \cos\left(\frac{u_{IM}(t)}{2V_\pi} \pi\right). \quad (2.39)$$

In (2.39), the phase modulator driving signals $u_{PM_1}(t) \dots u_{PM_{m-1}}(t)$ are again defined by (2.30) with $n = \{1..(m-1)\}$. The electrical driving signal for intensity modulation depends on the desired ring ratio, and is specified by

$$u_{IM}(t) = -\frac{2 \arccos\left(\frac{1}{RR}\right)}{\pi} \cdot V_\pi + \frac{2 \arccos\left(\frac{1}{RR}\right)}{\pi} \cdot V_\pi \cdot \sum_k (b_{m_k} \cdot p(t - kT_S)), \quad (2.40)$$

where $b_{m_k} \in \{0, 1\}$ corresponds to the last data bit of a symbol with m bits in the k -th symbol interval.

Similarly, the last phase modulator of the parallel DPSK transmitter, whose output signal is given by (2.33), can be replaced with an intensity modulator to obtain the *parallel Star QAM transmitter*. Its output signal is then given by

$$E_s(t) = \sqrt{P_s} \cdot e^{j(\omega_s t + \varphi_s)} \cdot a_{IQM}(t) \cdot e^{j\psi_{IQM}(t)} \cdot e^{j \frac{u_{PM_3}(t)}{V_\pi} \pi} \cdot \dots \cdot e^{j \frac{u_{PM_{m-1}}(t)}{V_\pi} \pi} \cdot \cos\left(\frac{u_{IM}(t)}{2V_\pi} \pi\right). \quad (2.41)$$

In Fig. 2.14, the eye diagrams of the normalized intensity, the IQ diagrams, and the chirp characteristics are depicted for the serial and the parallel Star 16QAM transmitter, considering NRZ and RZ pulse shapes and assuming a ring ratio of 1.8, a data rate of 40 Gbit/s and an electrical rise time of 1/4 of the symbol period.

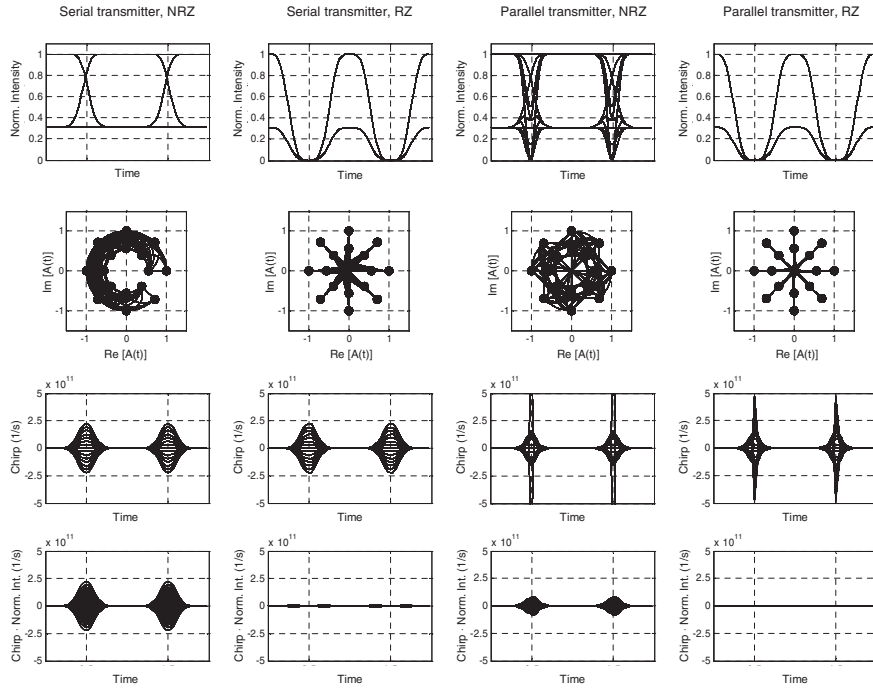


Fig. 2.14 Optical signal properties of different Star 16QAM transmitters

The same conclusions can be drawn as for 8DPSK. The impact of the chirp, which appears at the phase transitions, is reduced when the parallel configuration is employed, and is almost eliminated when RZ pulses are transmitted. This becomes apparent from the product of the chirp and the intensity (bottom diagrams in Fig. 2.14), introduced as an intuitive performance measure in Sect. 2.4.4.

2.6 Square QAM Transmitters

In Star QAM constellations described in the last section, first suggested by Cahn in 1960 [3], the same number of symbols is placed on different concentric circles. Star QAM signals can easily be generated by enhancing a phase modulation transmitter for an additional intensity modulation and can be differentially detected. On the other hand, these constellations are not optimal as regards noise performance, because symbols on the inner ring are closer together than symbols on the outer ring. In order to improve noise performance, Hancock and Lucky suggested placing more symbols on the outer ring than on the inner ring [5], leading to constellations with more balanced Euclidean distances. But they came to the conclusion that such systems are more complicated to implement. In 1962, the Square QAM constellation, shown in Fig. 2.15 for Square 16QAM, was introduced for the first time by Campopiano and Glazer [4]. Indeed, Square QAM signals are conveniently detected by coherent synchronous receivers and offer only a small improvement in noise performance, but—thinking in terms of two quadrature carriers—relatively simple modulation and demodulation schemes are possible, due to the regular structure of the constellation projected on the in-phase and quadrature axis. Today, the Square QAM is widely used in electrical systems. In optical transmission systems, however, it is still very distant from a commercial practical implementation.

The next sections illustrate *different transmitter options* for generating optical Square QAM signals, which are denoted here as “serial Square QAM transmitter”, “conventional IQ transmitter”, “enhanced IQ transmitter”, “Tandem-QPSK transmitter” and “multi-parallel MZM transmitter”. Each of these transmitters features different properties of its output signals and different complexities of its optical and electrical parts, which can be traded off. Detailed information about the electrical parts is provided, especially for two particular modulation formats: Square 16QAM, to which a special focus is brought in this book, and Square 64QAM, which is included here as a very ambitious format. Before going into the details of the transmitters, Sect. 2.6.1 outlines the differential quadrant encoding which must be employed for all transmitter configurations when the quadrant ambiguity arising at the carrier synchronization at the receiver shall be resolved through differential coding.

2.6.1 Differential Quadrant Encoding

A n times $\pi/2$ ($n = 0, 1, 2, 3$) phase ambiguity (quadrant ambiguity) arises at the carrier synchronization for synchronous detection of Square QAM signals, which can be resolved by so-called differential quadrant encoding. This encoding scheme combines a DQPSK encoding with a specific bit mapping, and was proposed by Weber in [22]. Two of the m bits of a Square QAM symbol determine the quadrant and are differentially encoded using a DQPSK differential encoder. This way, these two bits can be unambiguously recovered even if the absolute position of the received

constellation diagram is ambiguous with n times $\pi/2$. The remaining $(m - 2)$ bits can also be determined correctly for any n times $\pi/2$ rotation when the bit mapping is arranged as rotation symmetric with respect to these bits. As an undesired consequence, the bit mapping is then not further Gray coded, leading to an OSNR performance degradation compared with Gray coded bit mappings. Gray coded Square QAM signals can be received for instance when sending training sequences.

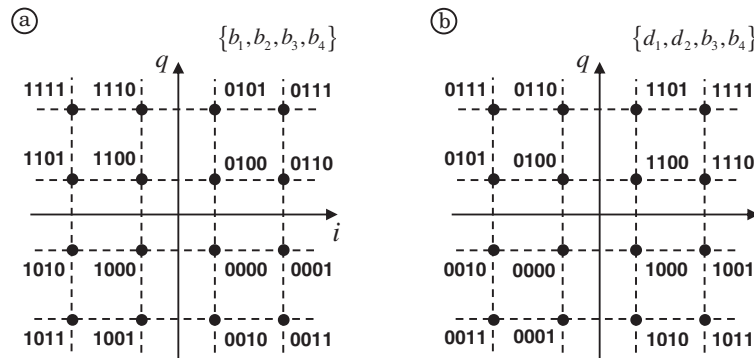


Fig. 2.15 a Bit mapping used for Square 16QAM, appropriate for differential quadrant encoding. b Symbol assignment after the DQPSK differential encoder.

Figure 2.15a shows a non Gray coded Square 16QAM bit mapping which is appropriate for differential quadrant encoding. It can be observed that any rotation of n times $\pi/2$ ($n = 0, 1, 2, 3$) causes no difference to the last two bits b_{3_k} and b_{4_k} . The first two bits, b_{1_k} and b_{2_k} , determine the quadrant and are encoded with a DQPSK differential encoder. When using the differential encoder of the parallel DQPSK transmitter described in Sect. 2.4.3, the differentially encoded bits d_{1_k} and d_{2_k} at the encoder output are assigned to the quadrants as illustrated in Fig. 2.15b.

2.6.2 Serial Square QAM Transmitter

In contrast to Star QAM constellations, the phases are arranged unequally spaced in Square QAM constellations, so that it is not possible to adjust all the phase states of the symbols by simply driving consecutive phase modulators with binary electrical driving signals. In [6], it was shown that any optical QAM signal can be generated by using a single dual-drive MZM (see Fig. 2.1b). In this case, however, the necessary number of states of electrical driving signals is quite high (e.g. 16-ary driving signals are needed for Square 16QAM), and a big electrical effort has to be engaged in to enable the simplicity of the optical part.

Another transmitter with a simple optical part capable of creating any QAM constellation is constituted by only two consecutive optical modulators: a MZM for adjustment of the amplitude state and a consecutive PM to set the phase. This transmitter is denoted as *serial Square QAM transmitter* throughout this book and is shown in Fig. 2.16. One more MZM can be employed for RZ pulse carving. The simplicity of the optical receiver part necessitates the use of a complex electrical level generator, since electrical driving signals with a high number of states must be generated (12-ary electrical driving signals are required for phase modulation in the case of Square 16QAM, for instance).

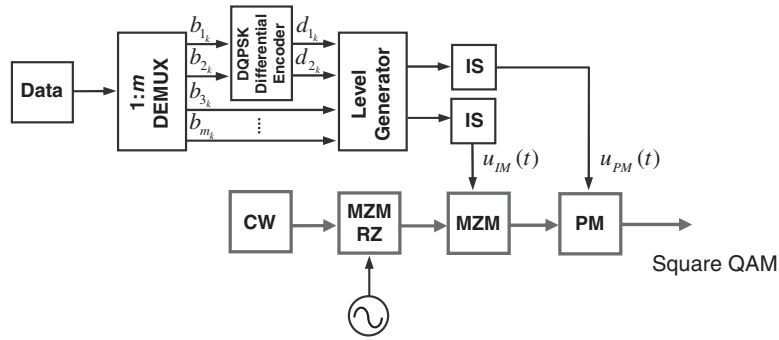


Fig. 2.16 Square QAM transmitter, serial configuration

The *optical output signal* of the serial Square QAM transmitter for NRZ pulse shape is given by

$$E_s(t) = \sqrt{P_s} \cdot e^{j(\omega_s t + \varphi_s)} \cdot \cos\left(\frac{u_{IM}(t)}{2V_\pi} \pi\right) \cdot e^{j \frac{u_{PM}(t)}{V_\pi} \pi}. \quad (2.42)$$

In order to adjust the desired amplitude and phase levels, the *multi-level electrical driving signals* for the MZM and the PM must be chosen as

$$u_{IM}(t) = -V_\pi + \frac{2V_\pi}{\pi} \cdot \sum_k \left(\arcsin\left(\frac{\sqrt{i_k^2 + q_k^2}}{\sqrt{2}}\right) \cdot p(t - kT_S) \right), \quad (2.43)$$

$$u_{PM}(t) = \frac{V_\pi}{\pi} \cdot \sum_k \left(\arg[i_k, q_k] \cdot p(t - kT_S) \right). \quad (2.44)$$

Equations (2.43) and (2.44) are generally applicable to any QAM constellation, and i_k and q_k represent the normalized symbol coordinates. For Square 16QAM, for instance, it holds $i_k \in \{-1, -1/3, 1/3, 1\}$ and $q_k \in \{-1, -1/3, 1/3, 1\}$, and the nor-

malized symbol coordinates i_k and q_k are related to the data bits $\{d_{1_k}, d_{2_k}, b_{3_k}, b_{4_k}\}$ as defined by the bit mapping shown in Fig. 2.15b and as specified in Table 2.3.

Table 2.3 Relation between the data bits $\{d_{1_k}, d_{2_k}, b_{3_k}, b_{4_k}\}$, the normalized symbol coordinates i_k and q_k , the normalized symbol amplitudes and the symbol phases for Square 16QAM after differential quadrant encoding for the bit mapping defined in Fig. 2.15b

d_{1_k}	d_{2_k}	b_{3_k}	b_{4_k}	i_k	q_k	Normalized amplitude	Phase ($^\circ$)
0	0	0	0	-1/3	-1/3	1/3	225
0	0	0	1	-1/3	-1	0.74	251.57
0	0	1	0	-1	-1/3	0.74	198.43
0	0	1	1	-1	-1	1	225
0	1	0	0	-1/3	1/3	1/3	135
0	1	0	1	-1	1/3	0.74	161.57
0	1	1	0	-1/3	1	0.74	108.43
0	1	1	1	-1	1	1	135
1	0	0	0	1/3	-1/3	1/3	315
1	0	0	1	1	-1/3	0.74	341.57
1	0	1	0	1/3	-1	0.74	288.43
1	0	1	1	1	-1	1	315
1	1	0	0	1/3	1/3	1/3	45
1	1	0	1	1/3	1	0.74	71.57
1	1	1	0	1	1/3	0.74	18.43
1	1	1	1	1	1	1	45

The arcsin-function in (2.43) makes sure to approach the appropriate intensity levels while taking the cosine field transfer function of the MZM into account. In [16], the electrical driving signals were classified as *ideal* and *non-ideal*. The so-called “ideal” driving signals, which are not very practical to generate, can be regarded as a theoretical approach to completely compensate for the MZM characteristic, so that the electrical pulse shape is directly transposed to the optical field amplitude. The “non-ideal” driving signals presented here yield correct intensity and phase states, but lead to small differences during the symbol transitions because they do not fully compensate for the cosine MZM characteristic. When observing (2.43), for instance, the corresponding “ideal” driving signal would be obtained by applying the arcsin-function to the whole sum. More details about this classification of the driving signals can be found in [16].

One of the main challenges for the practical implementation of the serial Square QAM transmitter is the generation of the multi-level electrical driving signals with an *electrical level generator*. The level-generator is located behind the differential encoder, as depicted in Fig. 2.16, and acts as a digital-to-analog converter. Figure 2.17 shows a possible setup of the level-generator for Square 16QAM, composed of AND-, NOR-, XOR- and XNOR-gates, an inverter, and attenuators. It illustrates the complexity of the electrical part in the serial Square QAM transmitter.

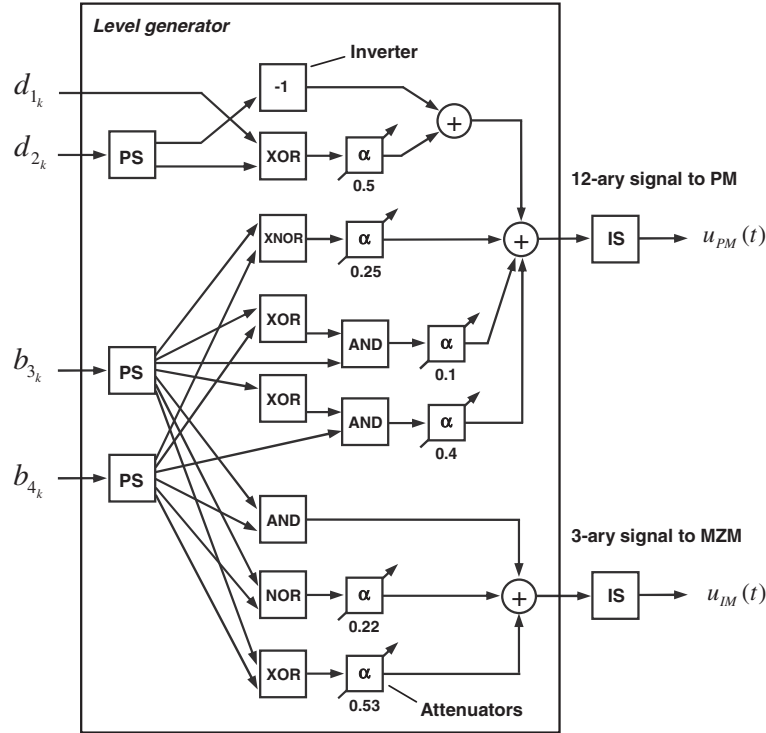


Fig. 2.17 Electrical level generator for the serial Square 16QAM transmitter, PS: power splitter

An optical Square 16QAM signal has 3 amplitude levels and 12 different phase states. The normalized amplitudes (given by $\sqrt{i_k^2 + q_k^2}/\sqrt{2}$) and phases ($\arg [i_k, q_k]$, in degrees) assigned to particular symbols after the differential encoder are listed in Table 2.3. When considering the generation of the 3-ary electrical driving signal for the MZM, the normalized amplitude is “1” if b_{3k} and b_{4k} are both logical one (application of an AND-gate), “1/3” if b_{3k} and b_{4k} are both logical zero (NOR-gate), and “0.74” if b_{3k} and b_{4k} are different (XOR-gate), respectively (see Table 2.3). This yields the configuration of the lower part of the level generator depicted in Fig. 2.17. The amplitude states of the MZM driving signal have to be further adjusted to compensate for the nonlinear MZM characteristic, resulting in the attenuation values shown in Fig. 2.17. For the generation of the 12-ary driving signal for the phase modulator, it can be observed from Table 2.3 that the phase is equal to 18.43° plus n times 90° if b_{3k} is logical one and b_{4k} is logical zero (realization by an XOR-gate and an AND-gate), equal to 45° plus n times 90° if b_{3k} and b_{4k} are both logical zero or both logical one (XNOR), equal to 71.57° plus n times 90° if b_{3k} is logical zero and b_{4k} is logical one (XOR, AND), and that d_{1k} and d_{2k} determine the quadrant,

and thus the value of n ($n = 0, 1, 2, 3$). To obtain a PM driving signal normalized to one, the appropriate values of the attenuators are also given in Fig. 2.17.

With the level generator described, the driving signals for the MZM and the PM are generated with the adequate relative values. It should be noted that the given attenuation values are only valid if the logical gates are operated with DC coupling at the outputs to obtain unipolar digital output signals. In practice, both signals must be amplified by modulator drivers to obtain the appropriate driving voltages for the modulators.

2.6.3 Conventional IQ Transmitter

It can be concluded from Sect. 2.6.2 that the serial Square QAM transmitter features a simple optical part, but requires a complex electrical level-generator which can not easily be implemented for high data rates. Due to the beneficial projection of the constellation points on the in-phase and quadrature axis, it is an advantage to generate square shaped constellations with IQ transmitters. This way, the number of states of the driving signals and thus the electrical complexity can effectively be reduced in comparison with the serial Square QAM transmitter. In Fig. 2.18, the setup of the conventional IQ transmitter for Square QAM is illustrated.

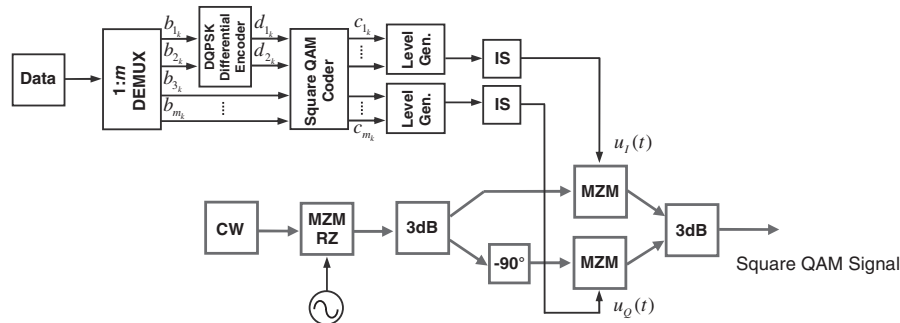


Fig. 2.18 Conventional IQ transmitter for Square QAM

The optical IQ modulator is also used within the parallel DPSK and Star QAM transmitter (see Sect. 2.4.2 and Sect. 2.5) to perform a DQPSK modulation. Whereas the in-phase and quadrature driving signals are binary for DQPSK, multi-level electrical driving signals are required to generate higher-order optical Square QAM constellations. The number of levels of the electrical driving signals is equal to the number of projections of the symbol points to the I-axis and the Q-axis (e.g. quaternary driving signals are required for Square 16QAM).